Applied Surface Science 544 (2021) 148583

Contents lists available at ScienceDirect

Applied Surface Science

journal homepage: www.elsevier.com/locate/apsusc

Full Length Article

# $TiO_2$ surface oxygen vacancy passivation towards mitigated interfacial lattice distortion and efficient perovskite solar cell

Hao Huang, Hejin Yan, Mingjun Duan, Jun Ji, Xin Liu, Haoran Jiang, Benyu Liu, Sajid Sajid, Peng Cui, Yingfeng Li, Meicheng Li *

*State Key Laboratory of Alternate Electrical Power System with Renewable Energy Sources, School of Renewable Energy, North China Electric Power University, Beijing 102206, China*

ARTICLE INFO

*Keywords:*
Perovskite solar cell
Surface oxygen vacancy
Interfacial interaction
DFT calculation

ABSTRACT

It is known that there exist inherent oxygen vacancies which is reported to be negative to PSCs performance on the $TiO_2$ film surface where contacts the gaseous phase while the manufacturing process. In this work, we clarified the role of surface oxygen vacancy on $TiO_2$/perovskite interface structure, which would not only serve as trap states to capture generated electrons, but also cause perovskite crystal distortion and Pb—I bond broken due to the interfacial interaction, generating additional interfacial defects. In addition, by analyzing the interfacial carrier transport routes, the common reason behind the different carrier loss pathways was ascertained to be the oxygen vacancy. Hence, for reducing oxygen vacancies and its negative impact on the device performance, the surface passivation method with gaseous fluorine was proposed, both the DFT (density functional theory) calculation results and experimental approaches proved that the surface passivation method could effectively reduce the traps states, mitigate interface structure distortion and enhance the interfacial charge transfer. As a consequence, $MAPbI_3$-based PSCs with surface passivation obtained a champion PCE of 20.43%, 7.7% higher than that (18.98%) of control device, and $FA_{0.15}MA_{0.85}PbI_3$-based PSCs with surface passivation obtained a champion PCE of 21.16%, 6.2% higher than that (19.92%) of control device.

## 1. Introduction

Due to the low-cost solution-processable manufacture and excellent photovoltaic performance, organic–inorganic metal halide perovskite solar cells (PSCs) show remarkable potential to be the most promising alternative to mitigate the excessive use of fossil fuels [1–5]. The first reported PSCs in 2009 only showed the power conversion efficiency (PCE) of 3.8% with terrible stability. With numerous studies carried out, researchers are making headway in the progress of PSCs, especially in its PCE, with the latest certificated efficiency of 25.2% [6–10]. Among the efficient planar PSCs, the most popular ETL is $TiO_2$ which has been applied in the PSCs in the initial period and received abroad attention in the past decade [11–13]. It is known that there exist inherent oxygen vacancies ($V_O$) on the $TiO_2$ film, especially on the film surface where contacts the gaseous phase while the manufacturing process. Within the n-i-p planar PSCs, the cell performance is closely related to the $TiO_2$/perovskite interfacial property which is strongly influenced by the surface oxygen vacancies. It is reported that the surface oxygen vacancies would serve as trap states to capture generated electrons and impact the adjacent perovskite structure due to interfacial interaction [14–16]. So based on the above thinking, to improve the cell performance, it is very important to optimize the $TiO_2$/perovskite interface structure and focus on the surface oxygen vacancy on the $TiO_2$ film surface.

To overcome the impact of $TiO_2$ surface defects on PSCs performance, surface/interface engineering is broadly applied. Introducing interfacial layer between the ETL and perovskite is an effective way to passivate the surface/interface defects and optimize the $TiO_2$/perovskite interface interaction. In 2018, Shi et al have reported that introducing a biopolymer heparin sodium (HS) interfacial layer into $MAPbI_3$ perovskite solar cell could boost the PCE from 17.2 to 20.1%, which mainly resulted from the passivation of ETL/perovskite interfacial traps through the interaction of the groups (—COO—, —$SO_3$, or $Na^+$) in HS with unpaired Pb and I in $MAPbI_3$ and $Ti^{4+}$-$V_O$ in $TiO_2$ [17]. Pointing at the defective metal oxide interface with the perovskite layer which is corresponded to a major limit for planar PSCs performance, a novel fulleropyrrolidine (NMBF-X, X = H or Cl) monomers and dimers were

* Corresponding author.
*E-mail address:* mcli@ncepu.edu.cn (M. Li).

https://doi.org/10.1016/j.apsusc.2020.148583
Received 26 August 2020; Received in revised form 4 November 2020; Accepted 21 November 2020
Available online 19 December 2020

designed and applied as an interfacial layer to passivate the interface trap states, and a maximum PCE of 22.3% was obtained [18]. However, although the interfacial layer showed its positive effect on interfacial defects passivation, the introduced layer would complex device structure and bring additional unknowable impacts. Except for the interfacial layer, the component tuning is also comprehensively explored as a potential approach to passivate the bulk/surface defects in the $TiO_2$ layer. For example, doping $TiO_2$ with a few amounts of Li [19], Nd [20], Nb [21], and NaCl [22] could reduce nonradiative recombination centers induced by oxygen vacancies, enhance electric conductivity, and then increase the photovoltaic metrics of the PSCs. Fluorine was broadly applied to passivate the oxygen vacancies as additive into precursor $TiO_2$ solution, and its positive passivation effects was proved in many reports, which demonstrated its potential to be the effective surface defects passivation approach [23–29]. Zhou et al have systematically explored the F doped $TiO_2$ applied in the PSCs and reported that the fluorine doping could inhibit the recombination of photogenerated electrons and holes and improve charge transfer [30,31]. However, as for the component tuning, it is hard to precisely control the amount of dopant and keep the integrity of intrinsic $TiO_2$ bulk crystal. So, it is necessary to design a novel way to target at the surface oxygen vacancies passivation in the $TiO_2$, and the interfacial interaction and charge transfer mechanism before or after passivation also need to be clarified.

Here, we proposed a surface oxygen vacancies targeted passivation method with gaseous fluorine on $TiO_2$ film. Based on the experimental approaches and DFT (density functional theory) calculation, the charge transfer and recombination mechanism at the interface with or without surface oxygen vacancy on $TiO_2$ film are explored, and the positive effects of fluorine passivated oxygen vacancy on interface structure interaction clarified. Due to the mitigated interfacial structure distortion and enhanced interfacial charge transfer, a champion PCE of 20.43% of the $MAPbI_3$ PSCs was obtained which is 7.68% higher than that (18.98%) of control device. It is also proved that the surface passivation method is suitable for $FA_{0.15}MA_{0.85}PbI_3$-based PSCs.

## 2. Results and discussion

In multilayered planar perovskite solar cells, the interface structure is very difficult due to the interfacial cooperated bond between different materials [32–34]. Inorganic metal oxide such as $TiO_2$ [35], ZnO [36], and $SnO_2$ [37] are commonly applied as ETL (electron transport layer) and the substrate of deposited perovskite film, which is unavoidable to cause a disharmonious interconnection and lattice distortion [38,39]. In addition, the interface defects resulted from lattice mismatch and distortion at the interface may impede charge transfer and accelerate ion migration and diffusion of oxygen and moisture, which may be responsible for the device instability [40]. So, it is necessary to consider the influence of bond interaction between different crystal structure when to estimate the interface property. Here, to explore the impact of $TiO_2$ surface oxygen vacancies on interface structure, we constructed interface crystal model with or without surface defects and then optimized using DFT calculation, the model parameters were presented in Table S1. As shown in Fig. 1a and b, At the $MAPbI_3/TiO_2(V_O)$ interface, the intrinsic surface defects, marked with bule circle, will not only

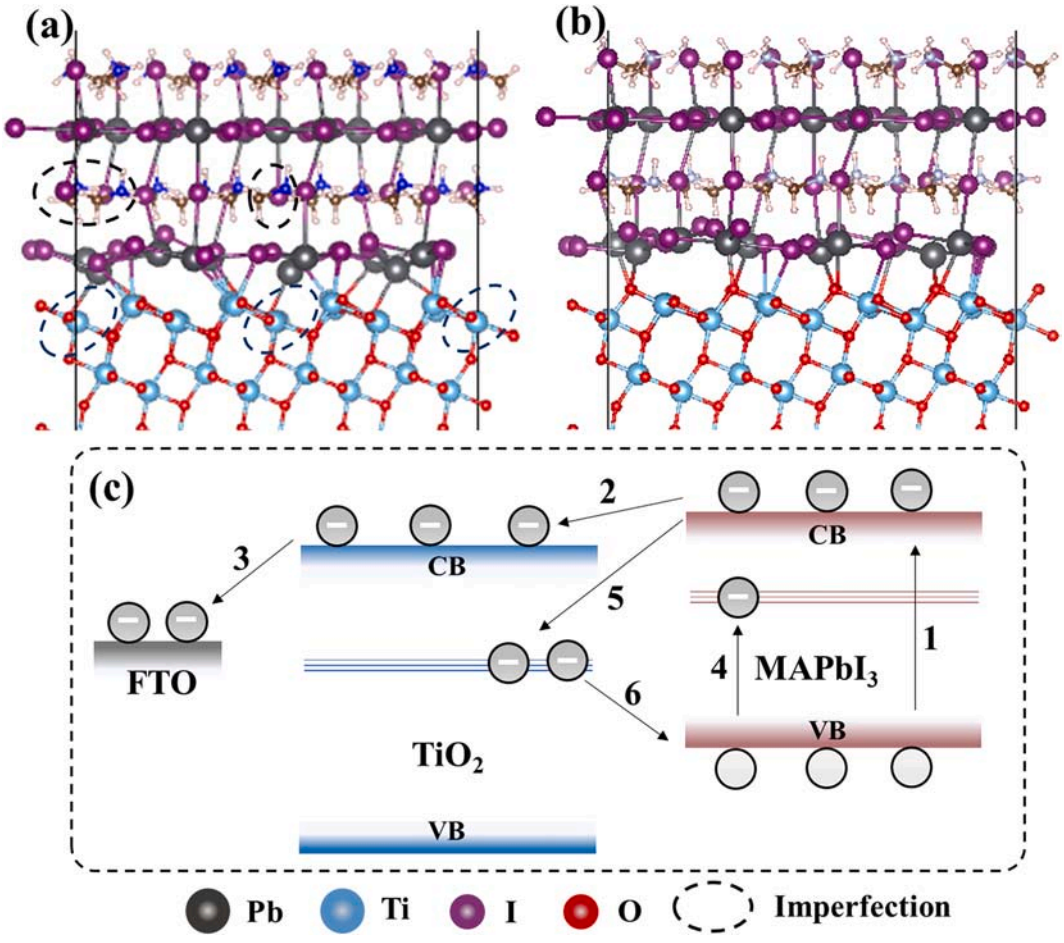


**Fig. 1.** Optimized interface structure and carrier transport process. (a) Optimized interface structure with surface defects in the $TiO_2$; (b) Optimized interface structure with perfect $TiO_2$; (c) Interface carrier transport process: 1. Generation; 2. Extraction; 3. Collection; 4. Trap-assisted electron capture within perovskite film; 5. Trap-assisted electron capture at the interface; 6. Trap-assisted recombination at the interface.

produce the trap level that captures generated electron from perovskite, but also will impact the adjacent perovskite crystal structure through the coordinated bonds. Due to the loss of O atoms on the surface of $TiO_2$, more Ti atoms were exposed in the surface which induced more Ti—I bonds formed. The increased Ti—I bonds would enhance the coordinate energy between the $TiO_2$ and terminal layer of perovskite film, and further to produce strain in the perovskite crystal. Meanwhile, because of the strong interaction between Pb atoms and O atoms at the interface, the original integrated terminal perovskite crystal structure would been destructed, the partial Pb—I bonds would been broken and the complete structure of the $PbI_5$ polyhedron would been distorted, which could generate undercoordinated I ions and $Pb^{2+}$ ions, the generated imperfection in the perovskite crystal due to the interfacial interaction were marked with black circle in Fig. 1a. The lattice distortion of microscopic crystal structure would produce a driving force for defect formation. For example, the broken I-Pb bond and distorted framework would tend to release the unbound I ions, producing I vacancy defects and I interstitial defects, which would create deep level traps within perovskite film [41,42]. In a comparison, in Fig. 1b. at $MAPbI_3/TiO_2$, the imperfection such as undercoordinated I ions and $Pb^{2+}$ ions had been effectively reduced and even eliminated.

From the bond perspective, comparing to $MAPbI_3/TiO_2(V_O)$ interface structure, the Ti—I bonds in the $MAPbI_3/TiO_2$ interface structure have obviously decreased which maybe the main reason for reduced interface interaction. And we also calculated the binding energy of $MAPbI_3/TiO_2$ is −3.86 eV, which is much bigger than that (−6.95 eV) of $MAPbI_3/TiO_2(V_O)$. So, based on the result of optimized interface structures analyzed above, the surface oxygen vacancies in $TiO_2$ film will not only produce trap level to capture electrons, but also will cause terminal perovskite crystal distortion and defect formation which is supposed to give rise to negative effects on perovskite optoelectronic properties. As shown in Fig. 1c, the carrier transport pathways were described with the situation of trap level in both $TiO_2$ and perovskite. It is obviously to see that the carrier loss mainly resulted from the path 4, 5 and 6. The trap level caused from interfacial interaction tends to capture photogenerated electrons within the perovskite film (path 4), and the captured electron is active that will further to recombine with the hole in the valence band (VB). Both the path 5 and 6 result from the intrinsic $TiO_2$ surface oxygen vacancy, the trap level in the $TiO_2$ would continuously capture the electron from the perovskite and recombine the hole in the perovskite VB, which dramatically reduced the collected carriers and PCE of PSCs [14,43,44]. It is not difficult to find that the original reason of the carrier loss is the $TiO_2$ surface oxygen vacancy which in charge of all the path 4, 5 and 6, the generated electron captured and recombined paths. So based on such thinking, for efficient PSCs, the $TiO_2$ surface oxygen vacancy is needful to be passivated.

Based on the mechanism of carrier dynamic at the interface between $TiO_2$ and perovskite mentioned above, targeting on the surface oxygen vacancies without any additional component and crystal structure changes inside the $TiO_2$ membrane, we proposed a surface passivation method in $TiO_2$, and which is proved to be compatible with the planar PSC fabrication method. As shown in Fig. 2, we firstly fabricated $TiO_2$ film on clean FTO substrate by chemical bath deposition method, then, we prepared a sealed chamber where contained a little diluted HF solution ($1 \times 10^{-4}$ M) whose acidity is too weak to damage $TiO_2$. We put the $TiO_2$/FTO sample into the chamber and keep it separated from the solution. Then, the chamber was heated with 120 °C for 2 h, generating the gas which included F to react with $TiO_2$, the surface undercoordinated Ti—$V_O$ is active to connect with F atom who exhibits strong capability of coordination. There are many previous reports to prove that the F could easily and successfully dope $TiO_2$ and occupy the O position in the $TiO_2$ crystal due to the higher reactivity and similar atomic size of O element, and in the field of materials engineering, the HF is a common dopant to fabricate F doped $TiO_2$ [45,46]. After the sample was taken out from the chamber, we washed it with ethyl alcohol and deionized water, and then dried it with nitrogen to keep sample clean for next step, we named the prepared $TiO_2$ as SP-$TiO_2$ (surface passivated $TiO_2$). The next step is the perovskite film fabrication, after

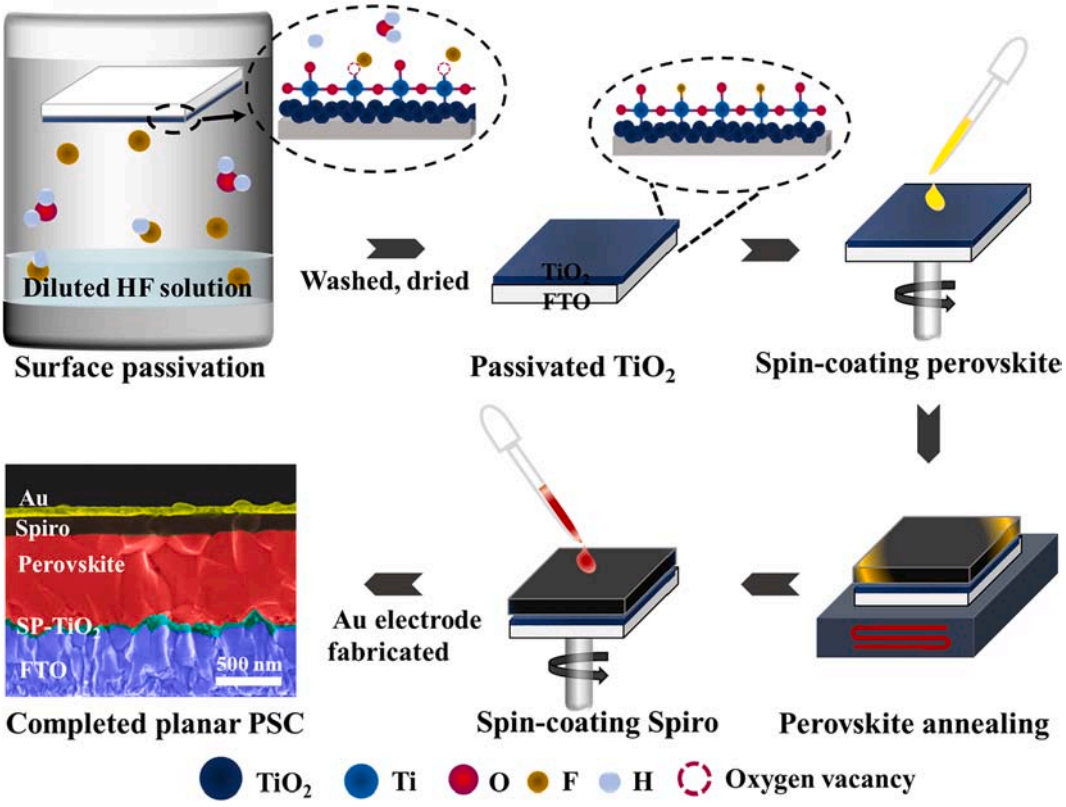


**Fig. 2.** Schematic of surface passivation method and PSC fabrication.

the sample treated with UV-ozone for 15 min, we carried out a one-step spin-coating with anhydrous ether as anti-solvent to prepare perovskite film, then the prepared film was heated at 130 °C for 15 mins. After it cooled to room temperature, the spiro-OMeTAD film was fabricated also by spin-coating on the perovskite film. Finally, about 60 nm Au electrode was prepared by vacuum evaporation. We performed the scanning electron microscopy (SEM) to observe the structure of PSCs that structured as FTO/SP-$TiO_2$/$MAPbI_3$/Spiro-OMeTAD/Au, the cross-section SEM image of the completed device was shown in Fig. 2, we found that each layer within the device was clear and labeled with white words, the SP-$TiO_2$ film was about 50 nm, and the perovskite film was about 600 nm.

To confirm the existence of F element on the $TiO_2$ film through passivating surface oxygen vacancies, we carried out the X-ray photoelectron spectroscopy (XPS) measurement to explore the existence of F element and its interaction with $TiO_2$. The corresponding original full XPS spectra of $TiO_2$ with or without surface passivation were presented in Fig. S1a, the analysis of element contents were shown in Fig. S1b and c. Compared to the XPS spectrum of control $TiO_2$, it is obviously to observe the peak of F 1s around 685 eV in the spectrum of SP-$TiO_2$, and in the both spectrum, the peaks of Ti 2p and O 1s almost share the same position and intensity which is consistent to the typical spectra of $TiO_2$. To observe the peak of F 1s clearer, we showed a precise map of XPS F 1s peak of SP-$TiO_2$ in Fig. 3a, it is clearer to confirm that the existence of F element. In detail, the high-resolution F 1s peak can be deconvoluted into two peaks located at 684 eV and 685.4 eV. The latter indicates that the F chemically bonded with Ti through forming a Ti—F structure [47–49]. Based on the surface crystal structure of $TiO_2$, the Ti—F structure could form from two ways, one is that the F filled O vacancy and connected with Ti—Vo, the unsaturated titanium atom. The second way is that the F replaced the O into the $TiO_2$ crystal. The latter way obviously needs more energy to take place, because it needs to break the Ti—O bond firstly. As inorganic metal oxide, the $TiO_2$ crystal structure is stable, which is difficult to be broken. So based on such theoretical analysis, the Ti—F structure is supposed to mainly come from the F connected with undercoordinated Ti—Vo on the $TiO_2$ film surface, which means the surface oxygen vacancies successfully passivated. The peak located at 684 eV can be assigned to F species physically absorbed on the surface of SP-$TiO_2$ based on the previous report [50]. As shown in Fig. 3b, comparing the Ti $2p_{2/3}$ peak of control $TiO_2$ film, we observed that the Ti $2P_{2/3}$ of SP-$TiO_2$ film shifts for 0.2 eV, which may result from the chemical interaction with the F during the surface passivation process and the appearance of Ti—F structure., which is in agreement with the results of precise map of XPS F 1 s peaks.

Many measurements were performed to explore the physical and optical properties of $TiO_2$ film with or without surface passivation, including X-ray diffraction (XRD), scanning electron microscopy (SEM), UV–Vis absorption and so on. As shown in Fig. 3c, the XRD spectra of control $TiO_2$ and SP-$TiO_2$ film were shown with the main peaks marked. The peaks of both films are almost share the same position with the similar intensity, and all the peaks are indexed to the typical diffraction peaks of $TiO_2$ film. To understand the influence of surface passivation on the film morphology, the SEM measurement was carried out to observe the samples. As shown in Fig. S2, we found that the impact of surface passivation on the film morphology is negligible, both the films are smooth and compact without any pinholes and cavities, which means the $TiO_2$ film has not been etched during the passivation method. The transmittance of ETLs should also be considered carefully, and the

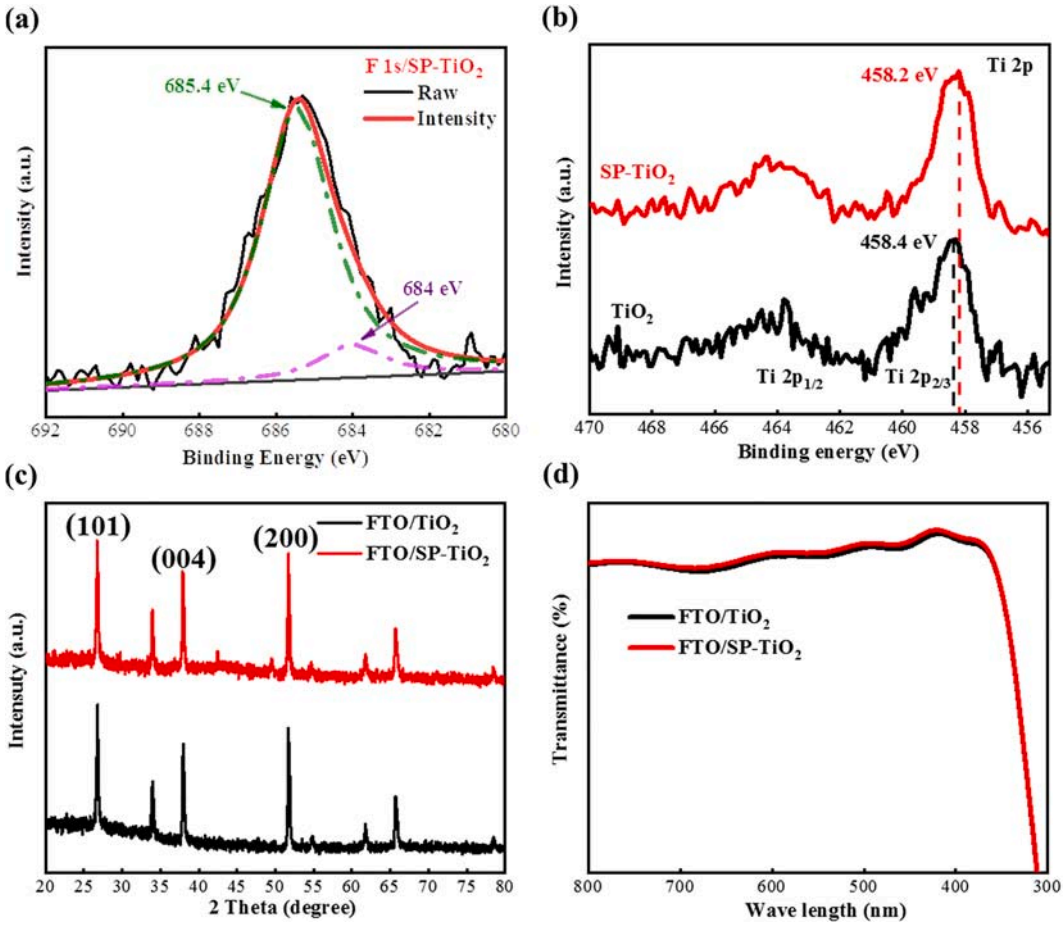


**Fig. 3.** Characterization of ETLs. (a) The F 1s XPS spectrum of ETL. (b) The Ti 2p XPS spectra of ETLs. (c) XRD spectra of ETLs. (d) Optical transmittance spectra of ETLs.

UV–Vis absorption was performed to explore the optical property of $TiO_2$ film and SP-$TiO_2$ film. As shown in Fig. 3d, we found that both the films possess excellent transmittance at visible range, and the transmittance of SP-$TiO_2$ is slightly superior than that of control $TiO_2$ film. The photos of $TiO_2$/FTO and SP-$TiO_2$/FTO samples were shown in Fig. S3, combining the UV–Vis absorption measurements and samples photos, we can find that the surface passivation method would not pollute and stain the $TiO_2$ film. All the results mentioned above indicated that the surface passivation method has beneficial effects on the property of $TiO_2$, and it is positively compatible with the fabrication method of planar n-i-p PSCs.

To explore the influence of the passivated oxygen vacancy with fluorine on the ETL/perovskite interface structure and interfacial electron extraction, the DFT calculation was carried out [51]. The optimized stable $MAPbI_3$/SP-$TiO_2$ heterostructure interfacial structure was shown in Fig. S4b and d, for the convenience of comparison, Fig. S4a and c showed the $MAPbI_3$/SP-$TiO_2$(Vo) heterostructure interface structure that has been once presented in Fig. 1a. Comparing to Fig. S4a, in the $MAPbI_3$/SP-$TiO_2$ heterostructure interface structure, the undercoordinated I ions were obviously decreased and even eliminated. Except for the reduced imperfection of the perovskite, the distortion of the perovskite terminal crystal lattice is obviously mitigated due to the F filled the oxygen vacancy. The structure parameters were shown in Table S2, the I—Ti bonds were obviously decreased and partial Pb atoms were connecting with F atom. We also calculated the binding energy of $MAPbI_3$/SP-$TiO_2$ is $-3.36$ eV/nm$^2$, which is apparently bigger than that ($-6.95$ eV/nm$^2$) of $MAPbI_3$/$TiO_2$($V_O$). Although the strong interface coordination is crucial for the structure stability, however, at the $MAPbI_3$/$TiO_2$(Vo) interface, due to the over-strong interaction, the perovskite crystal structure was destroyed, the framework was distorted, and the Pb—I bond was broken, which hugely reduced the structure stability and impeded charge transfer. To verify the surface Vo defects was effectively passivated, we calculated the trap level in both $MAPbI_3$/$TiO_2$(Vo) and $MAPbI_3$/SP-$TiO_2$, the projected density of states (PDOS) information was shown in Fig. 4a and b, in the $MAPbI_3$/$TiO_2$($V_O$), within both perovskite and $TiO_2$ bandgap, there exists trap level, which is consistent with the result analysis of Fig. 1. And in detail, as shown in Fig. S5a, the trap states widely distributed over the whole $MAPbI_3$/$TiO_2$(Vo) interface, which will serve as the carrier combination center in the process of interfacial charge transmission. In a comparison, in the $MAPbI_3$/SP-$TiO_2$, the trap level existed within $TiO_2$ bandgap is obviously mitigated, the trap density occupied at the trap level is much smaller than that of $TiO_2$(Vo), as shown in Fig. S5b, the negligible trap states located in a small area of the interface, which effectively reduces the impact of the defects on the interfacial charge transfer. As for the perovskite, the trap level is successfully eliminated, dramatically decreasing the generated electrons recombined within the perovskite film. We also calculated the $MAPbI_3$/$TiO_2$ (perfect) interface, as shown in Fig. S6, we can find that there is no trap level within both $TiO_2$ and perovskite bandgap, which further confirmed that the surface oxygen vacancies were mainly respond to the origin of interface trap states and the passivation method could effectively reduce the interface defects and nearly eliminate the defects resulted from nonideal interfacial interconnection in the perovskite film. In addition, the charge displacement curve (CDC) was calculated which is an available way to evaluate charge transport across the interface.[52] Firstly, we obtained the charge difference Δq between the interface, the formula was shown in the following:

$$\Delta q = \int_{-\infty}^{\infty}\int_{-\infty}^{\infty}(\rho_{ETL/MAPbI_3} - \rho_{ETL} - \rho_{MAPbI_3})d_x d_y$$

where $\rho_{ETL/MAPbI_3}$ is electron density of the interface, $\rho_{ETL}$ is electron density of ETL, $\rho_{MAPbI_3}$ is electron density of perovskite. The calculated

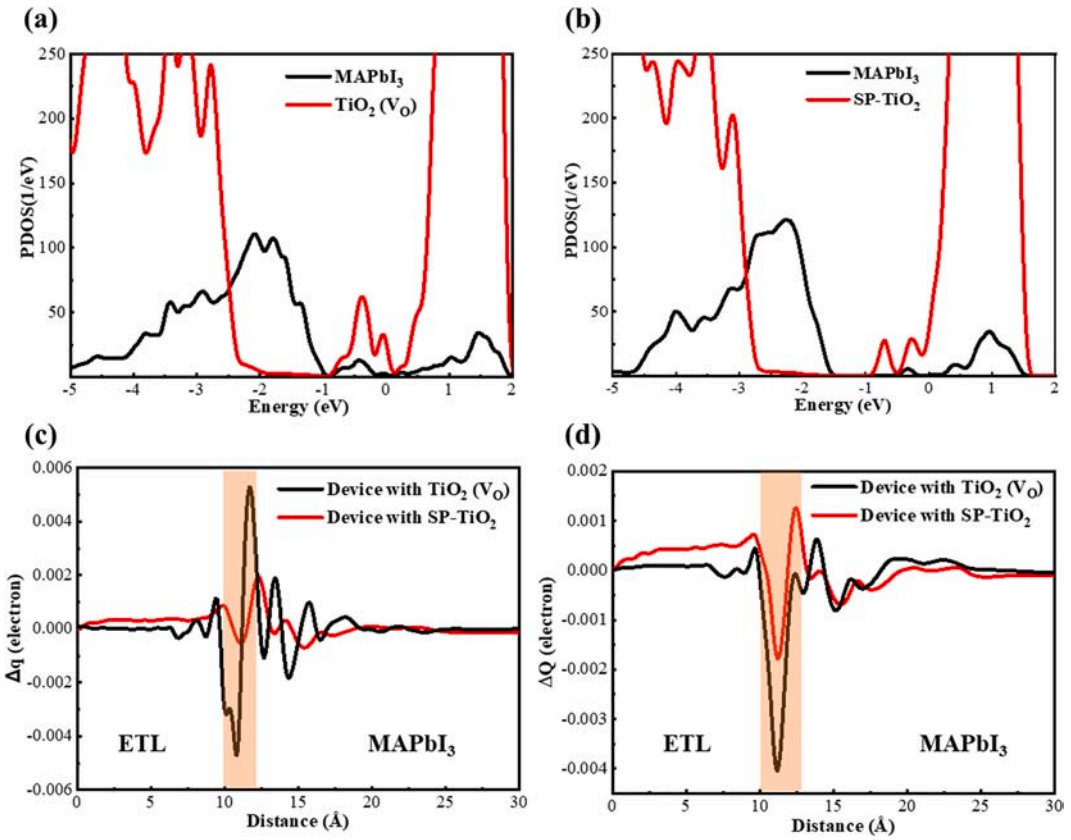


**Fig. 4.** Calculation of $MAPbI_3$/ETLs interfaces. (a) PDOS of $MAPbI_3$/$TiO_2$(Vo). (b) PDOS of $MAPbI_3$/SP-$TiO_2$. (c) Charge difference of devices. (d) Charge displacement curve of devices.

results of Δq was shown in Fig. 4c, we could find that both the device share the same trends of electron transport that the electron will accumulation at the interface. To clearly observe the interfacial charge transfer, we further obtained the CDC curves, the ΔQ could be calculated by integrating the charge difference Δq alone the z-direction to the interface, the formula was shown in the following:

$$\Delta Q = \int_{-\infty}^{z} \Delta q d_z$$

The CDC curves of devices was shown in Fig. 4d, the positive value in the CDC curve indicates that the charge transports from the right to the left. In the left part of the CDC curve of device with $TiO_2(V_O)$, the value is almost no change and close to zero, even to negative, which indicated that the electron extraction through $TiO_2(V_O)$ is weak, and partial electron transport from $TiO_2(V_O)$ to the perovskite. And at the interface, there accumulated mass of electron. Comparing to the CDC curve of device with $TiO_2(V_O)$, in the CDC curve of device with SP-$TiO_2$, except the small resign where located at the interface, the value of CDC in the whole region is positive which means that the charge was effectively transported from the perovskite to $TiO_2$. And we also could find that the interfacial electron accumulation was effectively alleviated. To intuitionally depict the charge transfer at the interface, the charge accumulation and deletion of the two interfaces was presented in Fig. S7, the red area represents charge accumulation and the green area represents charge extraction. We could find that there was more charge accumulated at the $MAPbI_3/TiO_2(V_O)$ interface, which is consistent with the CDC results.

Except for the DFT calculation, various experimental approaches were also carried out to explore the influence of surface passivation method on interfacial carrier dynamic and trap states. Before we investigate the ETL/perovskite interface property, we firstly analyzed the micro-morphology and crystallinity of perovskite film prepared on different ETLs through the SEM measurement. As shown in Fig. S8a and b, both the $TiO_2/MAPbI_3$ film and SP-$TiO_2/MAPbI_3$ film are compact and flat without pinholes, and both the average grain sizes are about 400 nm. We further carried out steady-state and time-resolved photoluminescence (PL and TRPL) measurements to explore the interface charge transfer. As shown in Fig. 5a, the PL intensity of perovskite film on control $TiO_2$ is obviously higher than that of perovskite film on SP-$TiO_2$ film, indicating that the carrier extracted from the perovskite film through SP-$TiO_2$ have increased. The results of TRPL were presented in Fig. 5b, we could find that the TRPL decay spectrum of the perovskite film is composed of fast decay component corresponding to the carrier fast decay lifetime τ1 and slow decay component corresponding to the carrier slow decay lifetime τ2. Previous studies of carrier decay reported that the fast decay component is mainly contributed to the interface carrier extraction. The τ1 of FTO/SP-$TiO_2/MAPbI_3$ is 11.89 ns which is almost half of that (22.58 ns) of FTO/$TiO_2/MAPbI_3$, indicating that the charge extraction at the SP-$TiO_2/MAPbI_3$ interface is very quick and the SP-$TiO_2$ film effectively facilitates the interfacial charge transport. Both the results of the PL and TRPL demonstrated that the surface passivation method applied on the $TiO_2$ ETL could facilitate interfacial charge transfer, which is consistent with conclusion of calculation. In addition, we fabricated the completed device to explore the interface trap states with or without surface passivation method. Firstly, we fabricated electron-only device to quantitatively evaluate the trap density of the devices [53], as shown in Fig. 5c, the device structure is FTO/ETLs/Perovskite/PCBM/Au. The defect density could be calculated by the

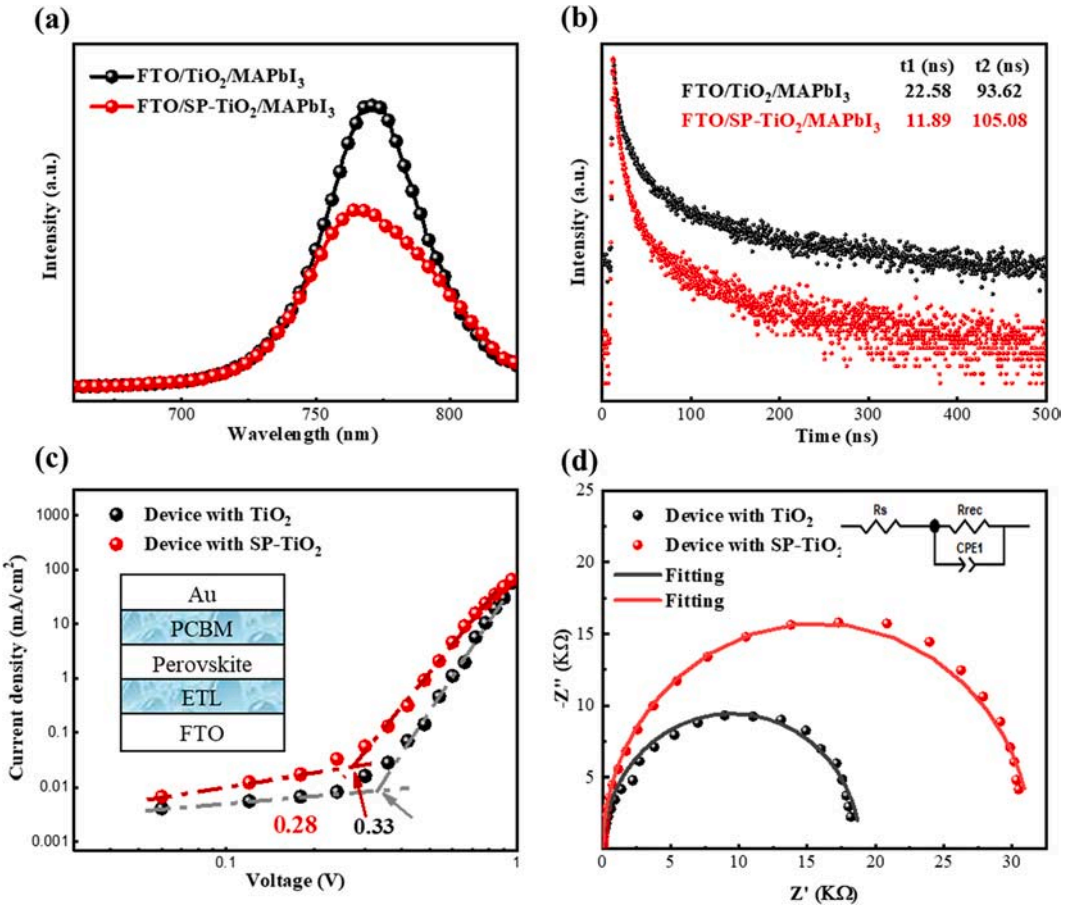


**Fig. 5.** The charge transfer and defects states at $MAPbI_3$/ETLs interfaces. (a) Steady-state PL spectra of $MAPbI_3$ films. (b) TRPL spectra of $MAPbI_3$ films. (c) Dark J-V curves of electron-only devices. (d) EIS spectra of devices.

equation:

$$N_{defects} = 2\varepsilon\varepsilon_0 V_{TEL}/eL^2$$

where the $\varepsilon$ is the relative dielectric constant of perovskite, according to the previous report, the value is 32 [54], $\varepsilon_0$ is the vacuum permittivity, the value is $8.85 \times 10^{-12}$ F/m, the e is the electron charge, the value is $1.6 \times 10^{-19}$ C, and the L is the thickness of the perovskite film, according to the cross-section SEM figure, the value is about 600 nm, and the $V_{TFL}$ is the trap-filled limit voltage which was presented in Fig. 5c. Both the device share the same $\varepsilon$, $\varepsilon_0$, e and L, we estimated the defect density to be $2.74 \times 10^{15}$ $cm^{-3}$ of device with SP-$TiO_2$, which is smaller than that ($3.24 \times 10^{15}$ $cm^{-3}$) of control device, indicating the interfacial defects within device has been effectively reduced due to the surface passivation method. The electrical impedance spectroscopy (EIS) is an effective approach to get insight observation of charge transfer and carrier recombination resistance information. The Nyquist plots and corresponding fitting curves of the devices with $TiO_2$ and SP-$TiO_2$ as ETL measured under reverse potential of 0.5 V and dark condition were presented in Fig. 5d. The $R_{rec}$ (resistance of recombination) is associated with the ETLs/perovskite interface since both the devices share the same perovskite/HTL interface. We found that the $R_{rec}$ of device with SP-$TiO_2$ is 31.5 KΩ which is obviously bigger than that (18.5 KΩ) of the control device, indicating that the carrier recombination is more difficult to take place and the carriers were more effectively transported and collected in the device with SP-$TiO_2$ [14,55]. The enhanced charge transport and suppressed carrier recombination are supposed to contribute to an outstanding device performance.

To check the influence of surface passivation method on the energy conversion efficiency (PCE) and verify its effect is universally appropriate for PSC with different perovskite materials composition, firstly $MAPbI_3$-based PSCs with and without surface passivation method were fabricated. For avoiding the damages of acid solution on $TiO_2$ film, we explored the effects of different HF solution diluted rate with deionized water during the surface passivation method on PSCs performance. As shown in Fig. S9 and Table S3, we kept the treated time with surface passivation is 1 h, it is obviously to find that the device obtained best performance with HF solution diluted rate is 200. Hereafter, the PSCs with SP-$TiO_2$ are fabricated with HF solution diluted rate is 200. In addition, we also explore the effects of treat time of surface passivation on performance of PSCs. As shown in Fig. S10 and Table S4, we could find that the device with best performance is obtained with 2 h, and when the treat time is 4 h, the PCE of PSCs began to decline slightly. Hereafter, the parameters of PSCs with SP-$TiO_2$ are obtained with treat time is 2 h. The J-V curves of champion $MAPbI_3$-based PSCs with and without surface passivation method were presented in Fig. 6a, it can be seen that the performance of device had been improved effectively with the surface passivation method applied on $TiO_2$. The PCE of PSCs tremendously increased from 18.98% (the control device without surface passivation) to 20.43% (device with surface passivation). It is notable to see the improvement of $J_{SC}$ that improved from 22.47 mA/$cm^2$ to 23.41 mA/$cm^2$, which mainly results from the enhanced extraction of carrier from perovskite to SP-$TiO_2$. Except the improvement of $J_{SC,}$ both the $V_{OC}$ and FF had slightly increased with the surface passivation, the FF has improved from 76.81% to 78.70%, and the $V_{OC}$ has improved from 1.09 V to 1.11 V. To verify the reproducibility of PSCs with SP-$TiO_2$, we analyzed parameters of 20 PSCs with and without

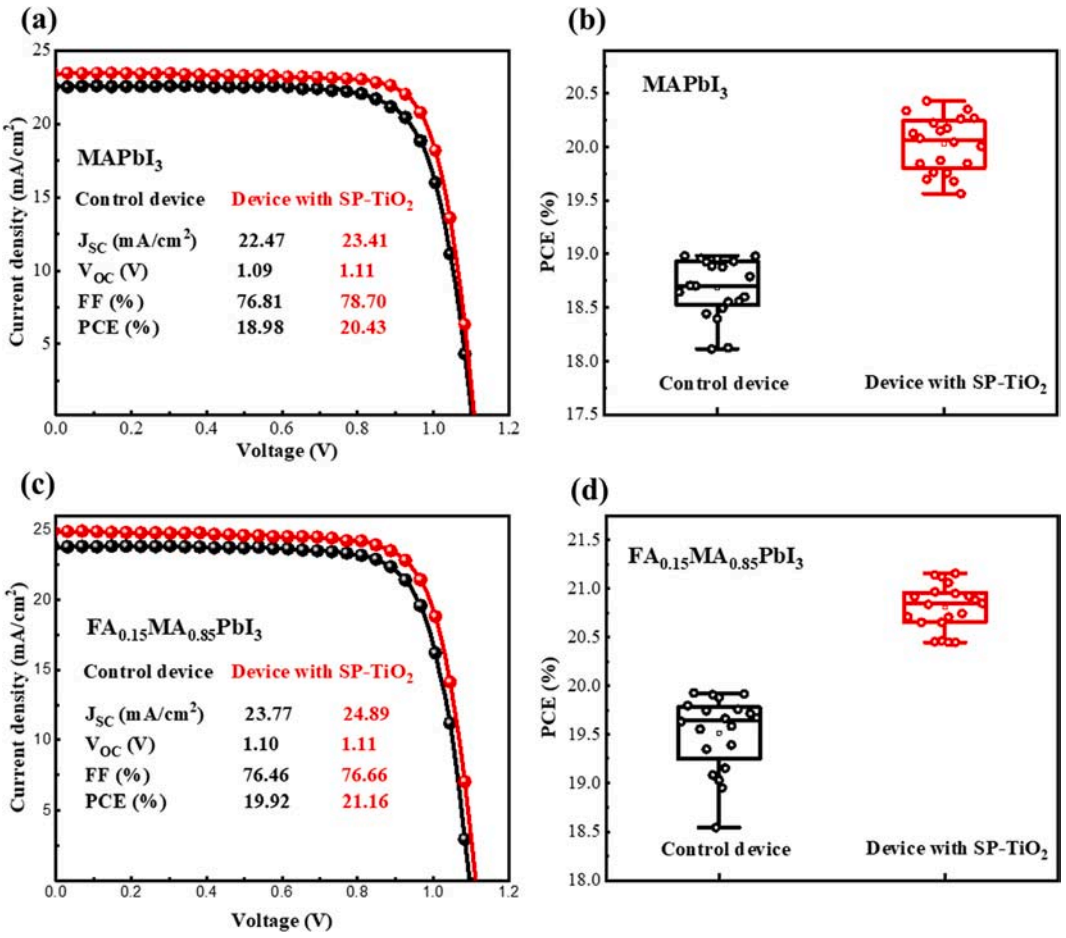


**Fig. 6.** Performance of devices. (a) J-V curves of champion $MAPbI_3$-baased devices. (b) Distribution of PCE. (c) J-V curves of champion $FA_{0.15}MA_{0.85}PbI_3$-baased devices. (d) Distribution of PCE.

surface passivation, respectively. Fig. 6b shows the distribution of PCE, and Fig. S11a–c shows the distribution of $J_{SC}$, $V_{OC}$ and FF, respectively. It apparently to see that the device with SP-$TiO_2$ exhibited a better performance and reproducibility compared to the control device, the average PCE of control devices is 18.68%, 7.4% lower than that (20.06%) of device with SP-$TiO_2$. And compared to the average FF of control devices, the average FF of device with SP-$TiO_2$ has improved from 75.60% to 77.41%.

The hysteresis of PSCs with or without surface passivation method was also explored, as shown in Fig. S11, we could find that the hysteresis of device with SP-$TiO_2$ get effectively mitigated, which mainly results from the reduced interfacial trap states and balanced charges transport [37,56]. Except the hysteresis, we further explored the stability of unencapsulated PSCs with or without surface passivation method, firstly, both the devices stored for 35 days in an ambient condition with about 50% humidity at room temperature, the PCE changes of both devices was recorded as shown in Fig. S12a, we can find that both the devices share the familiar decay trend, and although the stability of devices with SP-$TiO_2$ slightly improved compared to control device, the PCE was only 15.20% that retained 78.1% of original PCE after 35 days, the optimized $TiO_2$/perovskite interfacial interconnect may just slow the $H_2O$, $O_2$ molecular get into the perovskite film which badly influenced its stability, but cannot keep the perovskite film from outside environment. The UV stability of $TiO_2$-based PSCs is an important issue, so we also explored the influence of surface passivation method on devices UV stability. The unencapsulated device with SP-$TiO_2$ and control device were stored under 254-nm UV irradiation with an intensity of 50 $mW*cm^{-2}$ at room temperature in an argon-filled glovebox, the PCE decay curves were exhibited in Fig. S13, we could find that PCE decay of device with SP-$TiO_2$ was obviously slower than that of control device, especially in the later period since irradiation under UV light for 15 days, the PCE of device with SP-$TiO_2$ could retains 87.3% of original PCE after 35 days, in comparison, the PCE of control device could only retains 78.6% of original PCE after 35 days. It is also apparently to notice that the decay rate of device with SP-$TiO_2$ is much smaller than that of control device, which further to confirm the positive effects of surface passivation method on UV stability. The main reason of improved stability may the reduced $TiO_2$ surface oxygen vacancy that strongly influence the photocatalytic properties of the $TiO_2$. However, although the surface passivation method exhibited positive effects on PSCs stability, especially under the UV condition, the device after surface passivation method is still not stable enough to be applied, the stability of PSCs still needs to be further cared and explored.

The $FA_{0.15}MA_{0.85}PbI_3$-based PSCs with SP-$TiO_2$ and $TiO_2$ were also prepared, the J-V curves of champion devices were presented in Fig. 6c, the PCE of device with SP-$TiO_2$ is 21.16% which is 6.2% higher than that (19.92%) of control device. To further demonstrate the reproducibility of $FA_{0.15}MA_{0.85}PbI_3$-based PSCs with SP-$TiO_2$, we collected the cell performance parameters of 20 PSCs with SP-$TiO_2$ and $TiO_2$ respectively, Fig. 6d shows the distribution of PCE, and Fig. S14a–c shows the distribution of $J_{SC}$, $V_{OC}$ and FF, respectively. We can find that the PCE of control device broadly distributed in the range from 18.55% to 19.92%. In comparison, the PCE of devices with SP-$TiO_2$ distributed narrowly in the range from 20.45% to 21.16%, which exhibited an excellent reproducibility. The average PCE is 20.80%, 6.5% higher than that (19.53%) of control devices. The FF of device with SP-$TiO_2$ is also effectively improved, and the average FF of devices with SP-$TiO_2$ is 76.53% which is obviously higher than that (75.07%) of control devices. All the results proved that the surface passivation method applied on the $TiO_2$ could effectively improve the device performance, which mainly resulted from the reduced $TiO_2$/perovskite interface defects, optimized interfacial lattice distortion and impeded carrier recombination.

## 3. Conclusion

In summary, the influence of surface oxygen vacancies on interface structure and carrier dynamic was clarified, which would not only form trap level to capture the generated electron and increase carrier recombination, but also would give rise to perovskite crystal distortion and Pb—I bond broken, producing defects assisted trap level in the perovskite. For avoiding the negative effects of surface oxygen vacancy on PSCs performance, a surface passivation method with gaseous fluorine was proposed, both the experimental research and DFT calculation results proved that the surface passivation could effectively reduce interface defects, alleviate crystal structure distortion, and enhance the interfacial charge transfer. The positive effects of surface passivation method on improving PSCs performance were confirmed on $MAPbI_3$-based PSCs and $FA_{0.15}MA_{0.85}PbI_3$-based PSCs. We believe that the mechanism of surface oxygen vacancy impacted interface structure and carrier transfer can also be a reference to other $TiO_2$-based devices, and the surface passivation method proposed in this work could be suitable for large area $TiO_2$-based PSCs and other optoelectronic application.

## Declaration of Competing Interest

The authors declare that they have no known competing financial interests or personal relationships that could have appeared to influence the work reported in this paper.

## Acknowledgment

This work is supported partially by National Natural Science Foundation of China (Grant nos. 51772096 and 51972110), Beijing Science and Technology Project (Z181100005118002), Par-Eu Scholars Program, Science and Technology Beijing 100 Leading Talent Training Project, the Fundamental Research Funds for the Central Universities (2017ZZD02) and the NCEPU “Double First-Class” Program.

## Appendix A. Supplementary material

Supporting Information is available free of charge on the website. The additional data needed to evaluate the conclusions are presented in the Supplemental Information, including SEM image, characterization of the ETLs, characterization of the perovskite films, characterization of devices performance. In addition, the experimental procedures and calculation procedures are also included in the Supplemental Information. Supplementary data to this article can be found online at https://doi.org/10.1016/j.apsusc.2020.148583.

## References

[1] N.J. Jeon, J.H. Noh, W.S. Yang, et al., Compositional engineering of perovskite materials for high-performance solar cells, Nature 517 (2015) 476–480.
[2] D. Wei, F. Ma, R. Wang, et al., Ion-migration inhibition by the cation–π interaction in perovskite materials for efficient and stable perovskite solar cells, Adv. Mater. 30 (31) (2018) 1707583.
[3] P. Cui, D. Wei, J. Ji, et al., Planar p-n homojunction perovskite solar cells with efficiency exceeding 21.3%, Nat. Energy 4 (2019) 150–159.
[4] E. Jia, D. Wei, P. Cui, et al., Efficiency enhancement with the ferroelectric coupling effect using P(VDF-TrFE) in $CH_3NH_3PbI_3$ solar cells, Adv. Sci. 6 (16) (2019) 1900252.
[5] S. Sajid, A.M. Elseman, D. Wei, et al., NiO@carbon spheres: a promising composite electrode for scalable fabrication of planar perovskite solar cells at low cost, Nano Energy 55 (2019) 470–476.
[6] A. Kojima, K. Teshima, Y. Shirai, et al., Organometal halide perovskites as visible-light sensitizers for photovoltaic cells, J. Am. Chem. Soc. 131 (17) (2009) 6050–6051.
[7] D. Wei, H. Huang, P. Cui, et al., Moisture-tolerant supermolecule for the stability enhancement of organic–inorganic perovskite solar cells in ambient air, Nanoscale 11 (3) (2019) 1228–1235.
[8] D.Y. Son, J.W. Lee, Y.J. Choi, et al., Self-formed grain boundary healing layer for highly efficient $CH_3NH_3PbI_3$ perovskite solar cells, Nat. Energy 1 (7) (2016) 16081.
[9] Q. Jiang, Y. Zhao, X. Zhang, et al., Surface passivation of perovskite film for efficient solar cells, Nat. Photonics 13 (7) (2019) 460–466.
[10] NREL Best Research-Cell Efficiency Chart, https://www.nrel.gov/pv/assets/pdfs/best-research-cell-efficiencies.20191106.pdf.

[11] H.S. Kim, N.G. Park, Parameters affecting I-V hysteresis of $CH_3NH_3PbI_3$ perovskite solar cells: effects of perovskite crystal size and mesoporous $TiO_2$ layer, J. Phys. Chem. Lett. 5 (17) (2014) 2927–2934.
[12] H.J. Snaith, A. Abate, J.M. Ball, et al., Anomalous hysteresis in perovskite solar Cells, J. Phys. Chem. Lett. 5 (9) (2014) 1511–1515.
[13] Y. Rong, Y. Hu, S. Ravishankar, et al., Tunable hysteresis effect for perovskite solar cells, Energy Environ. Sci. 10 (11) (2017) 2383–2391.
[14] J. Ji, X. Liu, H. Jiang, et al., Two-stage ultraviolet degradation of perovskite solar cells induced by the oxygen vacancy-$Ti^{4+}$ states, iScience 23 (4) (2020) 101013.
[15] J. Zhao, Y. Deng, H. Wei, et al., Strained hybrid perovskite thin films and their impact on the intrinsic stability of perovskite solar cells, Sci. Adv. 3 (11) (2017) eaao5616.
[16] T.W. Jones, A. Osherov, M. Alsari, et al., Lattice strain causes non-radiative losses in halide perovskites, Energy Environ. Sci. 12 (2) (2019) 596–606.
[17] S. You, H. Wan, S. Bi, et al., A biopolymer heparin sodium interlayer anchoring $TiO_2$ and $MAPbI_3$ enhances trap passivation and device stability in perovskite solar cells, Adv. Mater. 30 (22) (2018) 1706924.
[18] H. Wang, F.B. Li, P. Wang, et al., Chlorinated fullerene dimers for interfacial engineering toward stable planar perovskite solar cells with 22.3% efficiency, Adv. Energy Mater. 10 (21) (2020) 2000615.
[19] F. Giordano, A. Abate, J.P.C. Baena, et al., Enhanced electronic properties in mesoporous $TiO_2$ via lithium doping for high-efficiency perovskite solar cells, Nat. Commun. 7 (2016) 10379.
[20] B. Roose, K.C. Godel, S. Pathak, et al., Enhanced efficiency and stability of perovskite solar cells through Nd-doping of mesostructured $TiO_2$, Adv. Energy Mater. 6 (2) (2016) 1501868.
[21] B. Chen, H. Rao, W. Li, et al., Achieving high-performance planar perovskite solar cell with Nb-doped $TiO_2$ compact layer by enhanced electron injection and efficient charge extraction, J. Mater. Chem. 4 (15) (2016) 5647–5653.
[22] H. Li, D. Li, W. Zhao, et al., NaCl-assisted defect passivation in the bulk and surface of $TiO_2$ enhancing efficiency and stability of planar perovskite solar cells, J. Power Sources 448 (2020) 227586.
[23] D.B. Dwyer, D.J. Cooke, M.F. Hidalgo, et al., Fluorine doping of nanostructured $TiO_2$ using microwave irradiation and polyvinylidene fluoride, J. Fluorine Chem. 227 (2019) 109375.
[24] K. Lee, M. Hou, V. Suryanarayanan, et al., Sequential preparation of dual-Layer fluorine-doped tin oxide films for highly efficient perovskite solar cells, Chemsuschem 11 (18) (2018) 3234–3242.
[25] W. Ho, J.C. Yu, S. Lee, et al., Synthesis of hierarchical nanoporous F-doped $TiO_2$ spheres with visible light photocatalytic activity, Chem. Commun. 10 (2006) 1115–1117.
[26] D. Li, H. Haneda, S. Hishita, et al., Visible-light-driven N-F-codoped $TiO_2$ photocatalysts. 1. Synthesis by spray pyrolysis and surface characterization, Chem. Mater. 17 (10) (2005) 2588–2595.
[27] C. Yu, Q. Fan, Y. Xie, et al., Sonochemical fabrication of novel square-shaped F doped $TiO_2$ nanocrystals with enhanced performance in photocatalytic degradation of phenol, J. Hazard. Mater. 237 (2012) 38–45.
[28] M. Che, Y. Fang, J. Yuan, et al., F-doped $TiO_2$ compact film for high-efficient perovskite solar cells, Int. J. Electrochem. Sci. 12 (2017) 1064–1074.
[29] X. Zhang, Y. Wu, Y. Huang, et al., Effect of fluorine doped $TiO_2$ on the property of perovskite solar cell, Iop Conf. 182 (2017) 012001.
[30] X. Zhang, Y. Wu, Y. Huang, et al., Reduction of oxygen vacancy and enhanced efficiency of perovskite solar cell by doping fluorine into $TiO_2$, J. Alloys Compd. 681 (2016) 191–196.
[31] Y. He, Q. Yan, X. Liu, et al., Effect of annealing on the structure, morphology and photocatalytic activity of surface-Fluorinated TiO2 with dominant 001 facets, J. Photochem. Photobiol., A 393 (2020) 112400.
[32] M. De Bastiani, G. Dellerba, M. Gandini, et al., Solar cells: Ion migration and the role of preconditioning cycles in the stabilization of the J-V characteristics of inverted hybrid perovskite solar cells, Adv. Energy Mater. 6 (2) (2016) 1501453.
[33] L. Zuo, Q. Chen, N. De Marco, et al., Tailoring the interfacial chemical interaction for high-efficiency perovskite solar cells, Nano Lett. 17 (1) (2017) 269–275.
[34] R.A. Kerner, B.P. Rand, Linking chemistry at the $TiO_2/CH_3NH_3PbI_3$ interface to current-voltage hysteresis, J. Phys. Chem. Lett. 8 (10) (2017) 2298–2303.
[35] A.K. Chandiran, A. Yella, M.T. Mayer, et al., Sub-nanometer conformal $TiO_2$ blocking layer for high efficiency solid-state perovskite absorber solar cells, Adv. Mater. 26 (25) (2014) 4309–4312.
[36] P. Zhang, J. Wu, T. Zhang, et al., Perovskite solar cells with ZnO electron-transporting materials, Adv. Mater. 30 (3) (2018), 1703737.1–1703737.20.
[37] H. Huang, X. Liu, M. Duan, et al., Dual function of surface alkali-gas erosion on $SnO_2$ for efficient and stable perovskite solar cells, ACS Appl. Energy Mater. 3 (5) (2020) 5039–5049.
[38] C. Zhang, S. Yuan, Y. Lou, et al., Perovskite Films with Reduced Interfacial Strains via a Molecular-Level Flexible Interlayer for Photovoltaic Application, Adv. Mater. 2001479 (2020).
[39] Y. Che, Y. Lei, Y. Li, et al., Strain engineering and epitaxial stabilization of halide perovskites, Nature 577 (2020) 7789.
[40] Z. Zhu, Y. Bai, X. Liu, et al., Enhanced efficiency and stability of inverted perovskite solar cells using highly crystalline $SnO_2$ nanocrystals as the robust electron-transporting layer, Adv. Mater. 28 (30) (2016) 6478–6484.
[41] Y. Shao, Z. Xiao, C. Bi, et al., Origin and elimination of photocurrent hysteresis by fullerene passivation in $CH_3NH_3PbI_3$ planar heterojunction solar cells, Nat. Commun. 5 (2014) 5784.
[42] B. Chen, P.N. Rudd, S. Yang, et al., Imperfections and their passivation in halide perovskite solar cells, Chem. Soc. Rev. 48 (14) (2019) 3842–3867.
[43] J. Wang, W. Li, W. Yin, et al., Passivating detrimental DX centers in $CH_3NH_3PbI_3$ for reducing nonradiative recombination and elongating carrier lifetime, Adv. Mater. 32 (6) (2020) 1906115.
[44] Y. Li, J. Shi, B. Yu, et al., Exploiting electrical transients to quantify charge loss in solar cells, Joule 4 (2) (2020) 472–489.
[45] H.G. Yang, G. Liu, S.Z. Qiao, et al., Solvothermal synthesis and photoreactivity of anatase $TiO_2$ nanosheets with dominant 001 facets, J. Am. Chem. Soc. 131 (11) (2009) 4078–4083.
[46] M.V. Dozzi, C. Dandrea, B. Ohtani, et al., Fluorine-Doped $TiO_2$ materials: photocatalytic activity vs time-resolved photoluminescence, J. Phys. Chem. C 117 (48) (2013) 25586–25595.
[47] V. Singh, A. Rao, A. Tiwari, et al., Study on the effects of Cl and F doping in $TiO_2$ powder synthesized by a sol-gel route for biomedical applications, J. Phys. Chem. Solids 134 (2019) 262–272.
[48] S. Zhang, Q. Zhong, W. Zhao, et al., Surface characterization studies on F-doped $V_2O_5/TiO_2$ catalyst for NO reduction with $NH_3$ at low-temperature, Chem. Eng. J. 253 (2014) 207–216.
[49] Y. Zhang, C. Han, M.N. Nadagouda, et al., The fabrication of innovative single crystal N, F-codoped titanium dioxide nanowires with enhanced photocatalytic activity for degradation of atrazine, Appl. Catal., B 168–169 (2015) 550–558.
[50] W. Yu, X. Liu, L. Pan, et al., Enhanced visible light photocatalytic degradation of methylene blue by F-doped $TiO_2$, Appl. Surf. Sci. 319 (2014) 107–112.
[51] J. Haruyama, K. Sodeyama, I. Hamada, et al., First-principles study of electron injection and defects at the $TiO_2/CH_3NH_3PbI_3$ interface of perovskite solar cells, J. Phys. Chem. Lett. 8 (23) (2017) 5840–5847.
[52] H.J. Feng, W. Deng, K. Yang, et al., Double perovskite $Cs_2BBiX_6$ (B = Ag, Cu; X = Br, Cl)/$TiO_2$ heterojunction: an efficient Pb-free perovskite interface for charge extraction, J. Phys. Chem. C 121 (8) (2017) 4471–4480.
[53] D. Yang, X. Zhou, R. Yang, et al., Surface optimization to eliminate hysteresis for record efficiency planar perovskite solar cells, Energy Environ. Sci. 9 (10) (2016) 3071–3078.
[54] J. Chen, L. Zuo, Y. Zhang, et al., High-performance thickness insensitive perovskite solar cells with enhanced moisture stability, Adv. Energy Mater. 8 (23) (2018) 1800438.
[55] Z. Liu, K. Deng, J. Hu, et al., Coagulated $SnO_2$ colloids for high-performance planar perovskite solar cells with negligible hysteresis and improved stability, Angew. Chem. 58 (23) (2019) 11497–11504.
[56] E. Edri, S. Kirmayer, A. Henning, et al., Why lead methylammonium tri-iodide perovskite-based solar cells require a mesoporous electron transporting scaffold (but not necessarily a hole conductor), Nano Lett. 14 (2) (2014) 1000–1004.